How changes in the tilt angle of the geomagnetic dipole affect the coupled magnetosphere-ionosphere-thermosphere system

Ingrid Cnossen[1] and Arthur D. Richmond[1]

Received 21 June 2012; revised 27 August 2012; accepted 28 August 2012; published 12 October 2012.

[1] The orientation of the Earth's magnetic field has changed dramatically during the geological past. We have investigated the effects of changes in dipole tilt angle on the magnetosphere, ionosphere, and thermosphere, using the Coupled Magnetosphere-Ionosphere-Thermosphere (CMIT) model. The dipole tilt angle modulates the efficiency of solar wind-magnetosphere coupling, by influencing the diurnal variation in the angle μ between the dipole axis and the GSM z axis. This influences how much Joule heating occurs at high magnetic latitudes. The dipole tilt angle also controls the geographic distribution of the Joule heating, as it determines the geographic latitude of the magnetic poles. Changes in the amount and distribution of Joule heating with tilt an`gle produce further changes in temperature and neutral winds. The latter affect the O/N_2 ratio, which in turn modifies the peak electron density of the F_2 layer, N_mF_2. All these effects are most important when the Interplanetary Magnetic Field (IMF) is southward, while being almost negligible under northward IMF. However, a change in dipole tilt also changes the inclination of the magnetic field, which affects the vertical component of ionospheric plasma diffusion along the magnetic field, regardless of the IMF direction. Changes in vertical plasma diffusion are responsible for ~2/3 of the changes in N_mF_2 and most of the low to midlatitude changes in h_mF_2 under southward IMF and for most of the changes in both variables under northward IMF. Thermal contraction may be responsible for high-latitude decreases in h_mF_2 with increasing tilt angle under southward IMF.

Citation: Cnossen, I., and A. D. Richmond (2012), How changes in the tilt angle of the geomagnetic dipole affect the coupled magnetosphere-ionosphere-thermosphere system, *J. Geophys. Res.*, *117*, A10317, doi:10.1029/2012JA018056.

1. Introduction

[2] During the geological past, the orientation of the Earth's internal magnetic field has varied spectacularly, with complete magnetic field reversals occurring on average every few hundred thousand to every few million years [e.g., *Jacobs*, 1984]. In between full field reversals, geomagnetic excursions can occasionally take place. These are events during which at least one of the magnetic poles moves to a much lower geographic latitude than usual (at least 50°, sometimes even briefly crossing over to the opposite hemisphere [*Jacobs*, 1984]). Changes in the magnetic field on shorter timescales, e.g., ~10–1000 years, tend to be more subtle. For instance, the tilt of the geomagnetic dipole, by which we mean the angle between the best fitting dipole and the Earth's rotation axis, decreased from ~11.7° in 1960 to 10.5° in 2005, following a century of nearly no change in tilt angle [*Amit and Olson*, 2008].

[3] In this study we will investigate how changes in the dipole tilt angle from 0° to 60° affect the magnetosphere-ionosphere-thermosphere (MIT) system. The main aim of this work is to gain a better insight in the role of the dipole tilt angle in the MIT system and the mechanisms by which changes in tilt angle affect this system. This will help with understanding the effects of the more complex magnetic field changes that have occurred historically and complements two previous studies in which we examined the effects of changes in the dipole moment on the MIT system [*Cnossen et al.*, 2011, 2012]. A few simulations done with rather strong dipole tilts of 30°–60° are also interesting from a geological perspective, giving an idea of what the MIT system could be like during times of geomagnetic excursions, although in those cases the magnetic field is not necessarily dipolar. We will not consider here the extreme case of a tilt angle of 90° (dipole axis located in the equatorial plane), which was simulated by *Zieger et al.* [2004].

[4] This paper is organized as follows. In section 2 we will first consider from a theoretical perspective what the effects of a change in dipole tilt angle may be. This will serve as background when interpreting the results from the model simulations. A description of the model and the settings used specifically for this study are given in section 3. The results are presented in section 4, which is split into three sections. Section 4.1 is concerned with hemispheric and global mean

[1]High Altitude Observatory, National Center for Atmospheric Research, Boulder, Colorado, USA.

Corresponding author: I. Cnossen, High Altitude Observatory, National Center for Atmospheric Research, Boulder, CO 80301, USA. (icnossen@ucar.edu)

0148-0227/12/2012JA018056

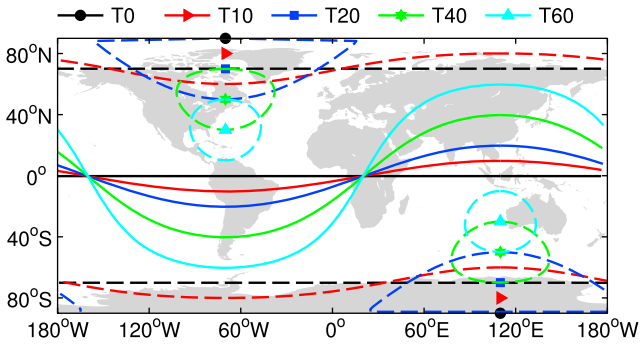

Figure 1. The locations of the magnetic poles (markers), the approximate locations of the polar caps (dashed lines), and the location of the magnetic equator (solid lines) for tilt angles of 0, 10, 20, 40 and 60° (labeled as T0, T10, etc.). The longitude of the Northern Hemisphere (NH) magnetic pole was set to 70°W in all cases, and correspondingly, the longitude of the Southern Hemisphere (SH) magnetic pole was set to 110°E. The polar caps were approximated as circles with a 20° radius around the magnetic poles (distortion of the circular shape is due to the projection).

responses to changes in tilt angle, and diurnal and seasonal variations in those, while section 4.2 focuses on the spatial structure of the responses. In section 4.3 we consider how the sign of the B_z component of the Interplanetary Magnetic Field (IMF) influences the results. A discussion of the results with a summary of our main conclusions is given in section 5.

2. Effects of Changes in Tilt Angle: Theory

[5] First, we consider the influence of the dipole tilt angle on the efficiency of the coupling between the solar wind and the magnetosphere. I. Cnossen et al. (The effects of seasonal and diurnal variations in the Earth's magnetic dipole orientation on solar wind-magnetosphere-ionosphere coupling, submitted to *Journal of Geophysical Research*, 2012) showed that the strongest coupling tends to occur when the dipole axis is aligned with the geocentric solar magnetospheric (GSM) z axis, with progressively weaker coupling taking place as the angle μ between these axes becomes larger. We remind the reader that the GSM y axis is defined as perpendicular to the dipole axis, so that the dipole axis is always contained in the x-z plane. The x axis points from the Earth to the Sun, which means that the angle μ between the dipole axis and the z axis varies both as a function of season and as a function of time of day, due to the angle between the Earth's equatorial plane and the ecliptic plane (~23.5°) and the angle between the Earth's rotation axis and the dipole axis (the dipole tilt), respectively. We note that μ is also sometimes referred to as "dipole tilt." However, in this study we will always consider "dipole tilt" to mean the angle between the Earth's rotation axis and the dipole axis. Since the dipole tilt influences how μ varies as a function of UT, a change in dipole tilt can modify the temporal variation in the efficiency of the coupling between the solar wind and the magnetosphere. In turn, a stronger solar wind-magnetosphere coupling will, in general, lead to a stronger magnetospheric driving of the polar ionosphere, which is associated with stronger ion flows and more Joule heating. As we shall see, this has consequences for the rest of the ionosphere-thermosphere system as well.

[6] A second, perhaps more obvious, effect of a change in tilt angle is that the geographic locations of the magnetic poles will change and with them the locations of the polar caps, where most of the coupling with the magnetosphere occurs. We define the polar caps here as the regions enclosed by the boundary between open and closed magnetic field lines, i.e., those connected to the IMF carried by the solar wind, and those that have both foot points on the Earth. The size of the polar caps can vary in response to variations in solar wind-magnetosphere coupling, but they are generally centered on the magnetic poles. The dipole tilt angle may therefore not only modulate the strength of the magnetospheric driving of the ionosphere, it also affects where this occurs geographically and thereby determines the location of the magnetospherically driven ionospheric convection patterns and the spatial distribution of energetic particle precipitation and Joule heating. Figure 1 shows schematically how changes in tilt angle between 0 and 60° affect the position of the magnetic poles and the approximate location of the polar caps. *Siscoe and Christopher* [1975] already pointed out that phenomena such as auroral displays, which we normally associate with high latitudes, could occur at much lower latitudes, given a large enough tilt angle. The interaction of polar cap phenomena with a low-latitude background thermosphere and ionosphere might also be different. In addition, the polar caps become associated with the specific longitudinal sectors in which the magnetic poles are located, which may result in more longitudinal variation in the ionosphere-thermosphere system.

[7] A third consequence of a change in tilt angle is the change in the orientation of magnetic field lines at a given geographic location. Field lines are by definition vertical at the magnetic poles and horizontal at the magnetic equator, with intermediate inclinations in between. The changes in the position of the magnetic equator with changing tilt angle were shown in Figure 1, and the circles that indicate the approximate location of the polar caps also represent a constant inclination contour. The orientation of the magnetic field is important for the ionosphere, because ionospheric plasma moves much more easily along field lines than across them. Changes in the inclination of the field can therefore change the vertical component of plasma transport, which is likely to affect key ionospheric parameters, such as the peak electron density of the F_2 layer, N_mF_2, and the height of the peak of the F_2 later, h_mF_2. Changes in the declination, the angle between the magnetic and geographic north direction, can also influence plasma transport, but this effect tends to be less important [*Cnossen and Richmond*, 2008].

3. Methodology

3.1. CMIT Model Description

[8] We examine the effects of changes in the dipole tilt angle using the Coupled Magnetosphere-Ionosphere-Thermosphere (CMIT) model [*Wiltberger et al.*, 2004; *Wang et al.*, 2004, 2008]. CMIT couples the Lyon-Fedder-Mobarry (LFM) global magnetospheric code [*Lyon et al.*, 2004] with the Thermosphere-Ionosphere-Electrodynamics General Circulation Model (TIE-GCM) [*Roble et al.*, 1988; *Richmond*

et al., 1992] through the MIX coupler module [*Merkin and Lyon*, 2010].

[9] The LFM component of the model solves the ideal magnetohydrodynamic (MHD) equations to simulate the interaction between the solar wind and the magnetosphere and calculates the full MHD state vector (plasma density, pressure, velocity, and magnetic field). It requires the solar wind MHD state vector on its outer boundary as input and uses an empirical parameterization [*Wiltberger et al.*, 2009] to calculate the energy flux of precipitating electrons. On its inner boundary it requires the ionospheric conductance to calculate the electric potential, which is passed in from the TIE-GCM part of the code through the MIX coupler module.

[10] The TIE-GCM is a time-dependent, three-dimensional model that solves the fully coupled, nonlinear, hydrodynamic, thermodynamic, and continuity equations of the thermospheric neutral gas self-consistently with the ion continuity equations. At high latitudes it requires the auroral particle precipitation and electric field imposed from the magnetosphere, which it receives from the MIX component of the code. The solar activity level is specified through an F10.7 value.

[11] The coupling of the LFM and TIE-GCM in CMIT enables the calculation of the global ionospheric electric field, which includes both the imposed high-latitude electric field from the magnetosphere and the dynamo electric fields generated by thermospheric winds. This makes CMIT a two-way coupled model, in which the magnetosphere is able to influence the ionosphere-thermosphere system and vice versa.

3.2. Simulation Setup

[12] We performed CMIT simulations using tilt angles of 0° to 60° at 10° increments, which will be referred to as T0, T10, T20, etc. The longitude of the geomagnetic pole in the Northern Hemisphere (NH) was kept fixed at 70°W, and the dipole moment was set to $8.0 \cdot 10^{22}$ A·m^2. All simulations were done for two seasons, each for a period of 36 h, starting at 0 UT on 21 March (equinox) or 21 June (solstice). The F10.7 value was set at 150 solar flux units (medium solar activity) and all simulations were done with the following idealized solar wind conditions. The solar wind density was set to a constant value of 5 cm^{-3}, and the outward solar wind speed was set to 400 km/s, while the speed in the GSM y- and z-direction was set to zero. The sound speed of the plasma in the solar wind was set to a constant 40 km/s, ensuring that the incoming solar wind was highly supersonic. The GSM B_z component of the IMF was set to −5 nT for the first 2 h (0–2 UT), +5 nT for the second 2 h (2–4 UT), and −5 nT for the rest of each simulation, while the GSM B_x and B_y components were set to zero for the full duration of the simulations. We note that in the geocentric solar ecliptic (GSE) coordinate frame, the B_y and B_z components vary over the course of a day (except for T0) with these settings. This study does therefore not consider diurnal variations associated with a modulation of the GSM B_y and B_z components as the Earth rotates, for a given GSE B_y and B_z. To test the influence of the sign of the IMF B_z component, we also performed the equinox T0 and T30 simulations with a solar wind that remained northward (+5 nT) from 2 UT onward, with all other settings the same as before.

[13] Only the last 24 h of each simulation were used for analysis since the first 12 h are required to reach a quasi-steady state. Some results are presented in the form of a mean with standard deviation over the last 24 h. With data output every 6 min, this gives 240 values for each calculation.

4. Results

4.1. Hemispheric and Global Mean Responses

[14] To understand the consequences of a change in dipole tilt angle, it is helpful to consider the angle μ between the GSM z axis and the dipole axis, which was introduced in section 2. We define μ as positive when the south magnetic pole, which is located in the Northern Hemisphere (NH), is inclined toward the Sun. As explained in section 2, we expect the coupling between the solar wind and the magnetosphere to maximize when $\mu = 0$ and gradually decrease as μ moves away from zero in either direction (for further details, see Cnossen et al., submitted manuscript, 2012). In general, the stronger the solar wind-magnetosphere coupling is, the higher the cross-polar cap potential is, although changes in the ionospheric conductance over the polar cap can modify this relationship slightly, with a higher conductance resulting in a lower cross-polar cap potential. The direction of the IMF, and in particular the sign of the B_z component, can also affect solar wind-magnetosphere coupling, which will be addressed to some extent in section 4.3. In this section and section 4.2 we will show results for southward IMF only.

[15] Figure 2a (top) shows the variation of μ as a function of UT during equinox for the different dipole tilts simulated here. For a zero dipole tilt, i.e., the case where the dipole axis is aligned with the Earth's rotation axis, $\mu = 0°$ throughout the day, but as soon as a nonzero dipole tilt is introduced, μ shows a semidiurnal variation, passing through 0° twice per day (at 10:40 and 22:40, as determined by the longitude of the geomagnetic poles). The larger the dipole tilt, the more the absolute value of μ, which we will refer to as μ_{abs}, deviates from 0° over the course of the day. This leads to correspondingly larger dips in the cross-polar cap potential (see Figure 2a (middle)), and a decrease in the 24-h average cross-polar cap potential (see Figure 3). The standard deviations over a 24-h period increase with increasing dipole tilt, representing an increase in diurnal variation.

[16] Figure 2b (top) shows the variation of μ as a function of UT during solstice. During solstice, as long as the dipole tilt angle is smaller than the angle between the Earth's equatorial plane and the ecliptic plane (∼23.5°), μ is closest to 0° just once per day (at 04:40 UT when the NH geomagnetic pole is located at 70°W). For larger dipole tilts (i.e., T30-T60), μ passes through 0° twice per day, but there is still a single point in time each day where μ is furthest away from 0°. At June solstice this occurs at 16:40 when the NH geomagnetic pole is located at 70°W. As one would expect, the two passes of μ through 0° for T30-T60 lead to a double peak in the cross-polar cap potential for those cases, while a single peak is seen for T10 and T20 (Figure 2b). All cases with nonzero tilt show a single minimum at 16:40 UT that gets deeper with increasing tilt angle. The average angle μ_{abs} over a 24-h period does not get considerably closer or further away from 0° as the tilt angle increases, and there is therefore not a clear trend in the average cross-polar cap potential with changing tilt angle during solstice (Figure 3). The standard deviation over a 24-h period does still increase with increasing tilt angle, as for equinox, reflecting the stronger diurnal variation.

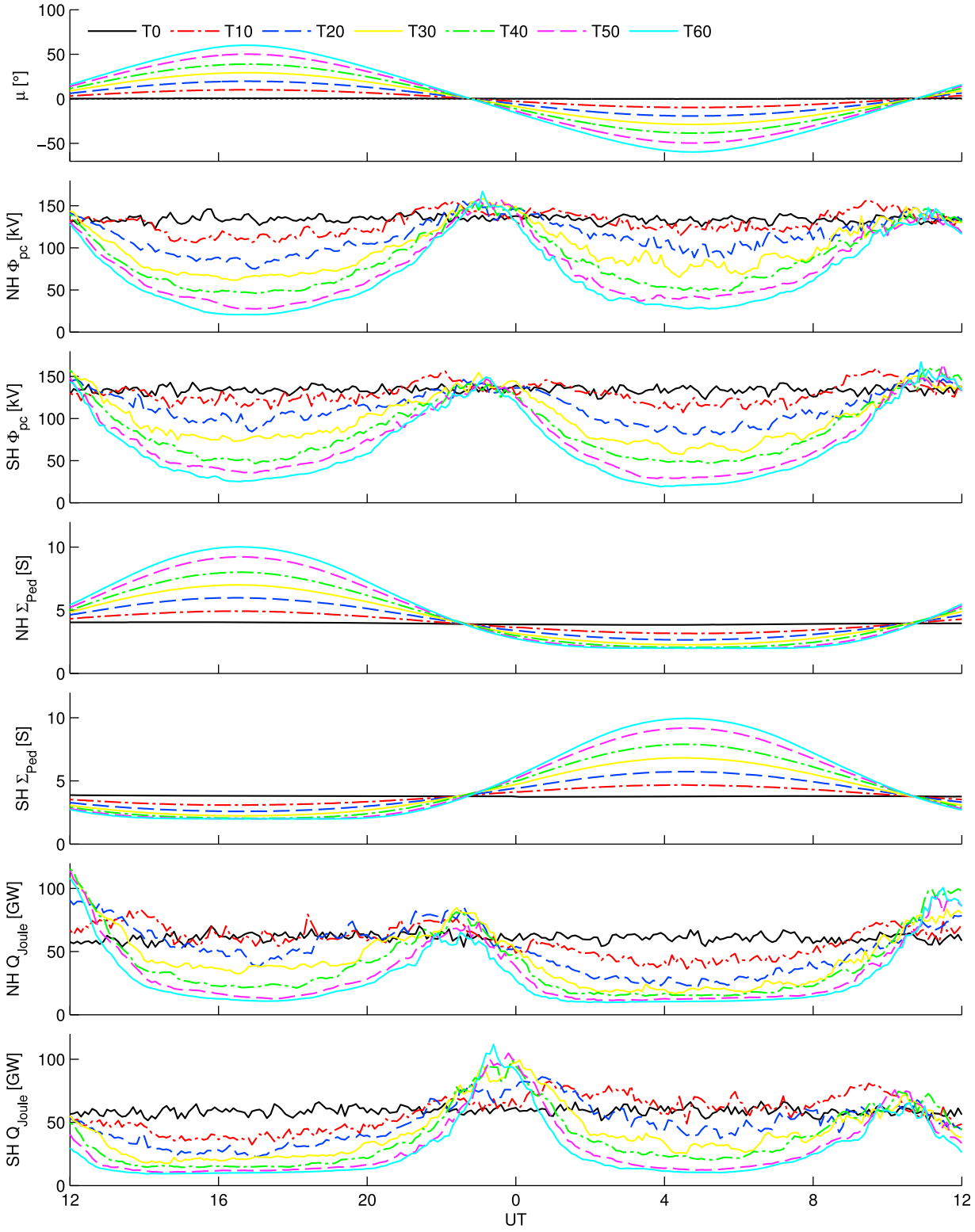

Figure 2a. The angle between the dipole axis and the GSM z axis, μ (°), the NH and SH cross-polar cap potential, Φ_{pc} (kV), the NH and SH Pedersen conductance, Σ_{Ped} (S), and the NH and SH integrated Joule heating power, P_{Joule} (GW) as a function of UT for tilt angles from 0 to 60° at March equinox. The Pedersen conductance is an average over magnetic latitudes >45°. The Joule heating power is evaluated over the full geographic hemispheres, although the main contribution is from high magnetic latitudes.

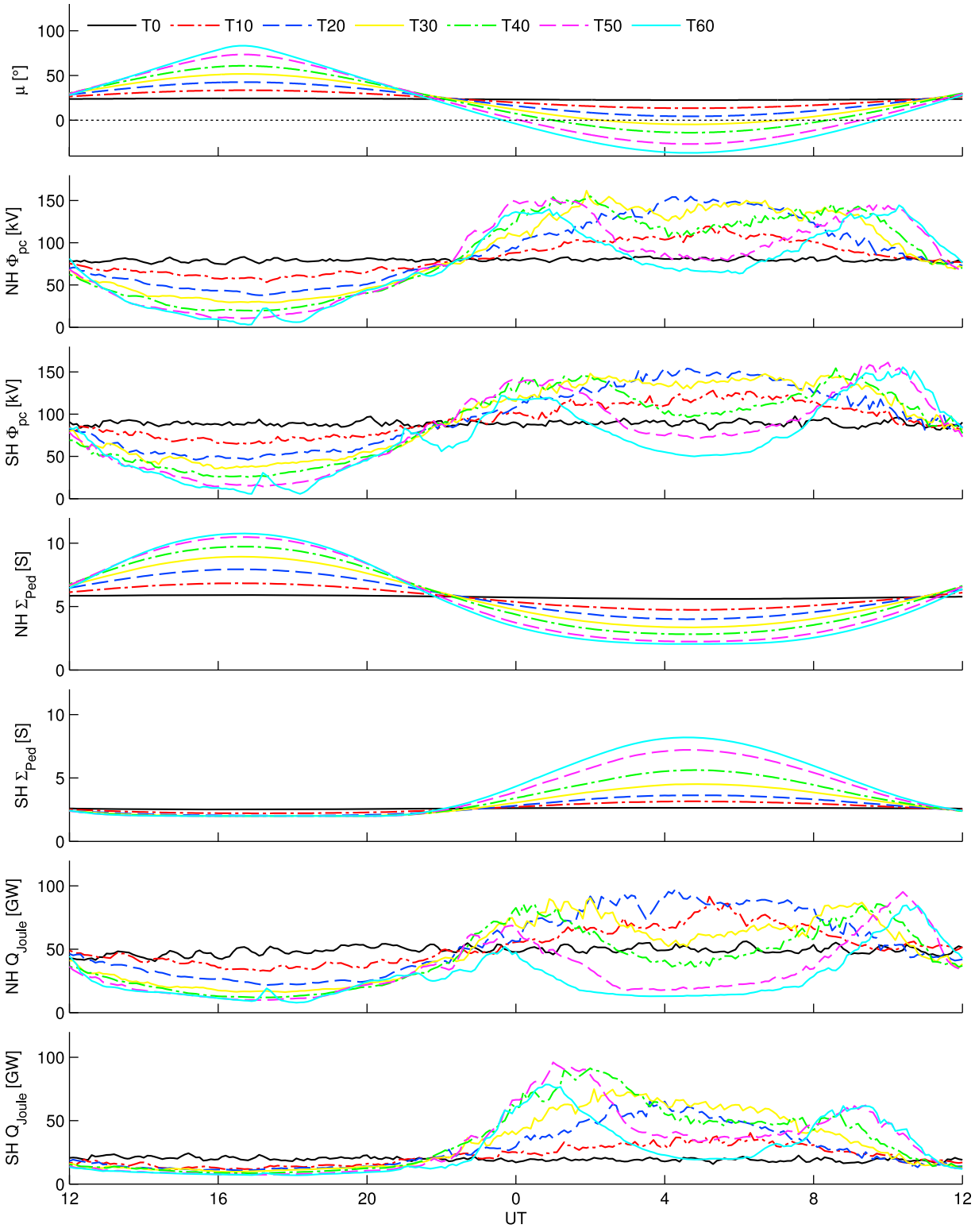

Figure 2b. Same as Figure 2a, but for June solstice.

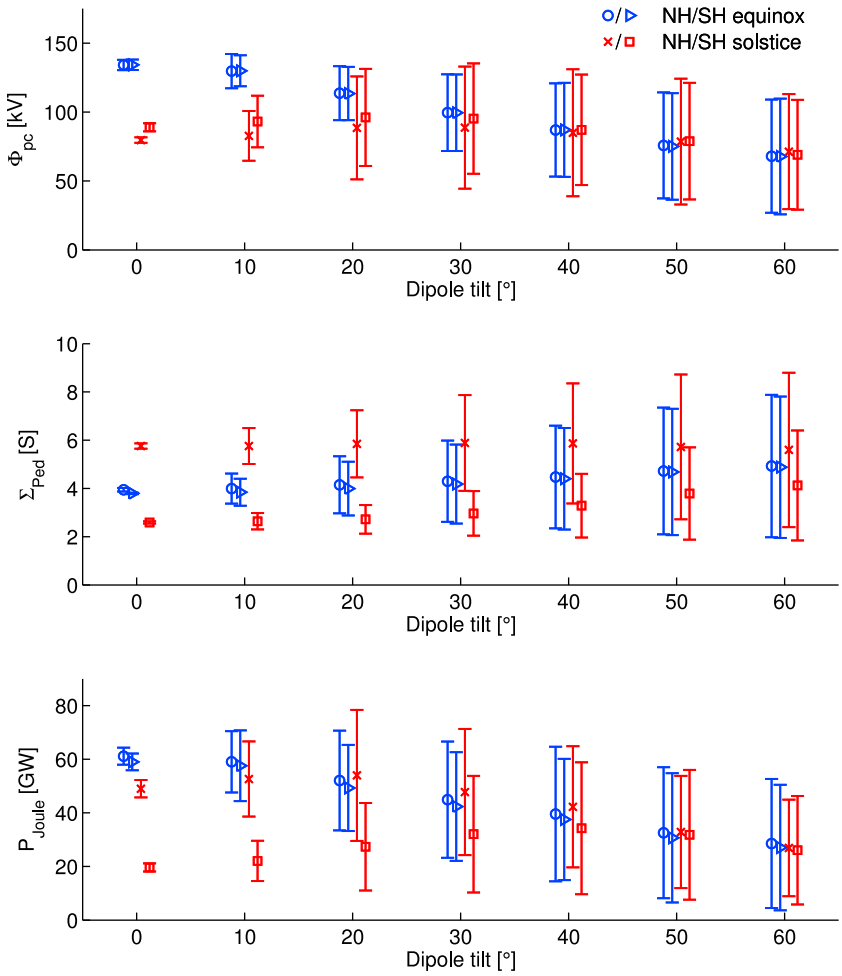

Figure 3. The 24-h mean cross-polar cap potential, Φ_{pc} (kV), Pedersen conductance, Σ_{Ped} (S), and Joule heating power, P_{Joule} (GW), as a function of dipole tilt angle, separated by hemisphere and season. The Pedersen conductance is an average over magnetic latitudes >45°. The Joule heating power is evaluated over the full geographic hemispheres, although the main contribution is from high magnetic latitudes. Plotted points have been offset to the left or right to avoid overlap.

[17] A reduction in solar wind-magnetosphere coupling is usually associated with both a decrease in cross-polar cap potential and a decrease in polar cap size. Indeed, we find that the polar cap area shows a similar diurnal variation as the cross-polar cap potential and on average decreases with increasing tilt angle (not shown). However, the variations in cross-polar cap potential are not fully balanced by the variations in polar cap size, so that they lead to variations in the electric field over the cross-polar cap, and variations in the corresponding ionospheric convection. The strength of the ionospheric convection determines in part how much Joule heating takes place, as can be seen from equation (1):

$$Q_J = \sigma_p B^2 \left[\left(U_e - U_{n,\perp}\right)^2 + \left(V_e - V_{n,\perp}\right)^2 + \left(W_e - W_{n,\perp}\right)^2 \right] \quad (1)$$

where Q_J is Joule heating per unit volume; σ_P is Pedersen conductivity; B is magnetic field strength; U_e, V_e, and W_e are the zonal, meridional, and vertical $\mathbf{E} \times \mathbf{B}$ drift velocities; and $U_{n,\perp}$, $V_{n,\perp}$, and $W_{n,\perp}$, are the zonal, meridional, and vertical components of the neutral wind velocity perpendicular to $\mathbf{B}$.

[18] On the other hand, the Joule heating is also influenced by the Pedersen conductivity (see equation (1)). The average ionospheric conductivity over the polar cap in a given hemisphere varies as a function of μ, being larger when the magnetic pole of the hemisphere in question is tilted more toward the Sun ($\mu > 0$ for the NH; $\mu < 0$ for the SH) due to higher ionization by solar radiation. The average Pedersen conductance (the vertically integrated conductivity) at high magnetic latitudes (>45°) is shown as a function of UT in Figures 2a (equinox) and 2b (solstice). The Hall conductance varies in a very similar way (not shown).

[19] Figures 2a and 2b also show the integrated Joule heating power in each geographic hemisphere as a function of UT. At equinox (Figure 2a), the diurnal variation of the Joule heating power is similar to the diurnal variation of the cross-polar cap potential, although the maximum around 23 UT tends to take place ~1 h earlier in the NH than in the SH. This is because the NH conductance is decreasing, while the SH conductance is increasing, around the time when the cross-polar cap potential maximizes. Similarly, the peak around 11 UT occurs earlier for the SH. The conductance

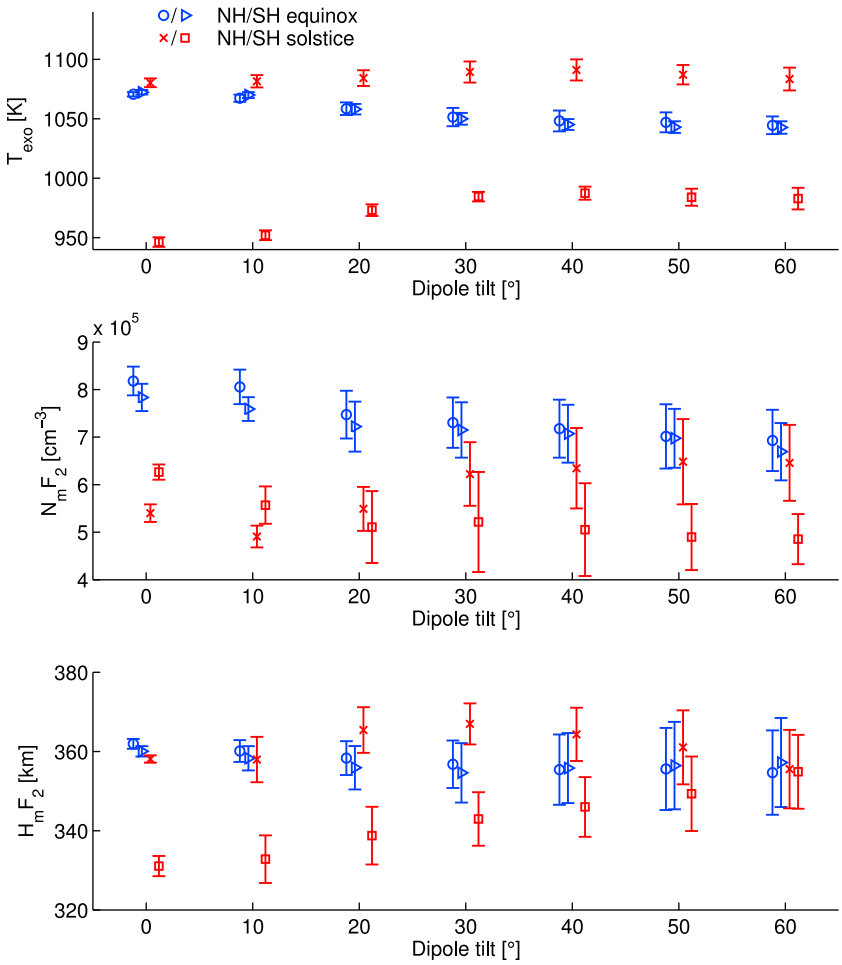

Figure 4. The 24-h mean exospheric temperature, T_{exo} (K), peak electron density of the F_2 layer, N_mF_2 (cm^{-3}), and height of the peak of the F_2 layer, h_mF_2 (km), as a function of dipole tilt angle, separated by hemisphere and season. All averages are done over geographic hemispheres. Plotted points have been offset to the left or right to avoid overlap.

thus modulates the diurnal variation in the Joule heating such that its periodicity becomes slightly shorter in the sunlit hemisphere. The minima in the sunlit hemisphere are also slightly less deep than the minima in the hemisphere tilted away from the Sun.

[20] At solstice (Figure 2b), the difference in conductance between the two hemispheres is more pronounced than it is at equinox, and the diurnal variation in the cross-polar cap potential is also different. In both hemispheres the cross-polar cap potential minimizes at 16:40 UT, but in the NH (summer) this is combined with high conductance and in the SH (winter) with low conductance. The Joule heating power in the SH therefore remains low almost regardless of the dipole tilt during the ~8 h around 16:40 UT, while in the NH the minima are deeper for larger dipole tilt, following the behavior of the cross-polar cap potential. For T10 and T20, there is a single peak in the cross-polar cap potential at 04:40 UT, which is larger for T20 than T10, and for both cases the conductance at high magnetic latitude is still slightly higher for the NH than the SH. This means that the peak in the NH Joule heating is also larger than the peak in the SH, and the peaks are larger for T20 than for T10. For T30–60 the structure becomes more complicated because of the double crossings of the $\mu = 0$ point. In the NH, the variation in Joule heating power more or less follows the variation in the cross-polar cap potential, but in the SH the first $\mu = 0$ crossing yields a more pronounced peak in the Joule heating power than the second one. It may not be directly clear why this is the case because the conductance at both $\mu = 0$ crossings is the same. However, after the first $\mu = 0$ crossing, the neutrals get accelerated by the high ion velocities, through ion-neutral collisions. That means that at the second $\mu = 0$ crossing, the neutral velocities are already relatively high, so that the difference between neutral and ion velocities is smaller. This makes the second peak in the Joule heating smaller (see equation (1)).

[21] Figure 3 summarizes how the 24-h mean values and standard deviations of the cross-polar cap potential, the Pedersen conductance, and the Joule heating depend on the tilt angle. The differences between the seasons (NH spring, SH fall, NH summer, and SH winter) become smaller with increasing tilt angle for all variables shown. For fall and spring this means a reduction in the cross-polar cap potential and Joule heating with increasing tilt angle, while for summer and winter these quantities initially increase but eventually decrease slightly with increasing tilt angle as well. For the

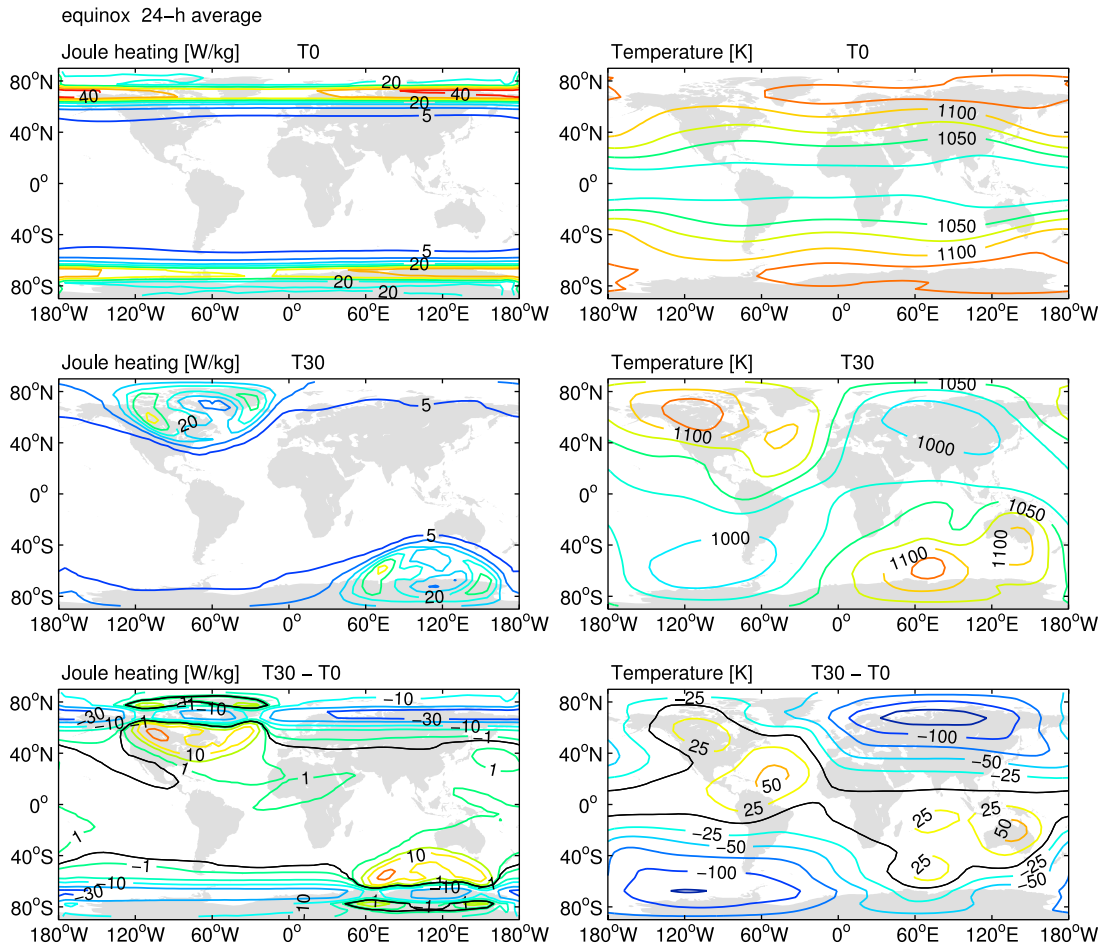

Figure 5. Maps of the 24-h mean Joule heating (W/kg) and temperature (K) for T0, T30, and the difference (T30-T0) for March equinox and southward IMF. All maps are at a constant pressure level of $3.2 \cdot 10^{-8}$ hPa, corresponding roughly to the level of the F_2 peak height.

Joule heating, this decrease starts at lower tilt angle, and is more pronounced for the summer hemisphere than for the winter hemisphere so that the initially larger Joule heating in the summer hemisphere reaches a similar level to the Joule heating in the winter hemisphere once a tilt angle of 50° is reached.

[22] We note that the cross-polar cap potentials simulated by CMIT tend to be too high compared to observations [*Wiltberger et al.*, 2004], probably because the region-2 current system is not very well represented [*Korth et al.*, 2004]. This could potentially result in the Joule heating being overestimated as well. However, a quick comparison of our Joule heating values with the ones observed by *McHarg et al.* [2005] shows that our values for the T10 case, which is closest to the present-day magnetic field configuration, fall well within the observed range. In particular the equinox and NH solstice values are close to the observed means for comparable solar wind conditions. The Joule heating therefore does not seem to be affected too much by the somewhat large cross-polar cap potentials.

[23] Figure 4 follows the format of Figure 3 but shows the hemispheric means of the exospheric temperature, the peak in the F_2 layer electron density, N_mF_2, and the height of the peak of the F_2 layer, h_mF_2, as a function of dipole tilt. The hemispheric mean exospheric temperature behaves in a way roughly similar to the Joule heating, and it is likely that the global mean temperature changes are mainly caused by changes in the energy input from the magnetosphere, as reflected in the Joule heating. Changes in exospheric temperature are largest in the SH solstice case (winter) for the relatively low dipole tilts, which is probably due to the relatively more important role of Joule heating in this case compared to other seasons, when solar radiation will be relatively more important.

[24] The hemispheric mean h_mF_2 appears to follow more or less the changes in the exospheric temperature, although there are some exceptions. For instance, the SH solstice h_mF_2 keeps increasing with increasing dipole tilt, while there is not much change anymore in the SH solstice temperature for tilts larger than 30°. It thus seems that thermal contraction/expansion may be responsible for some of the change in h_mF_2, but it is probably not the only process affecting h_mF_2. The same can be said about N_mF_2. N_mF_2 also shows similar behavior to the exospheric temperature for equinox, but for solstice it initially decreases with increasing dipole tilt in both hemispheres, while certainly the SH solstice temperature increases with increasing tilt. This indicates that other processes are probably contributing to changes in h_mF_2 and N_mF_2 as well, which will be explored further in the next section.

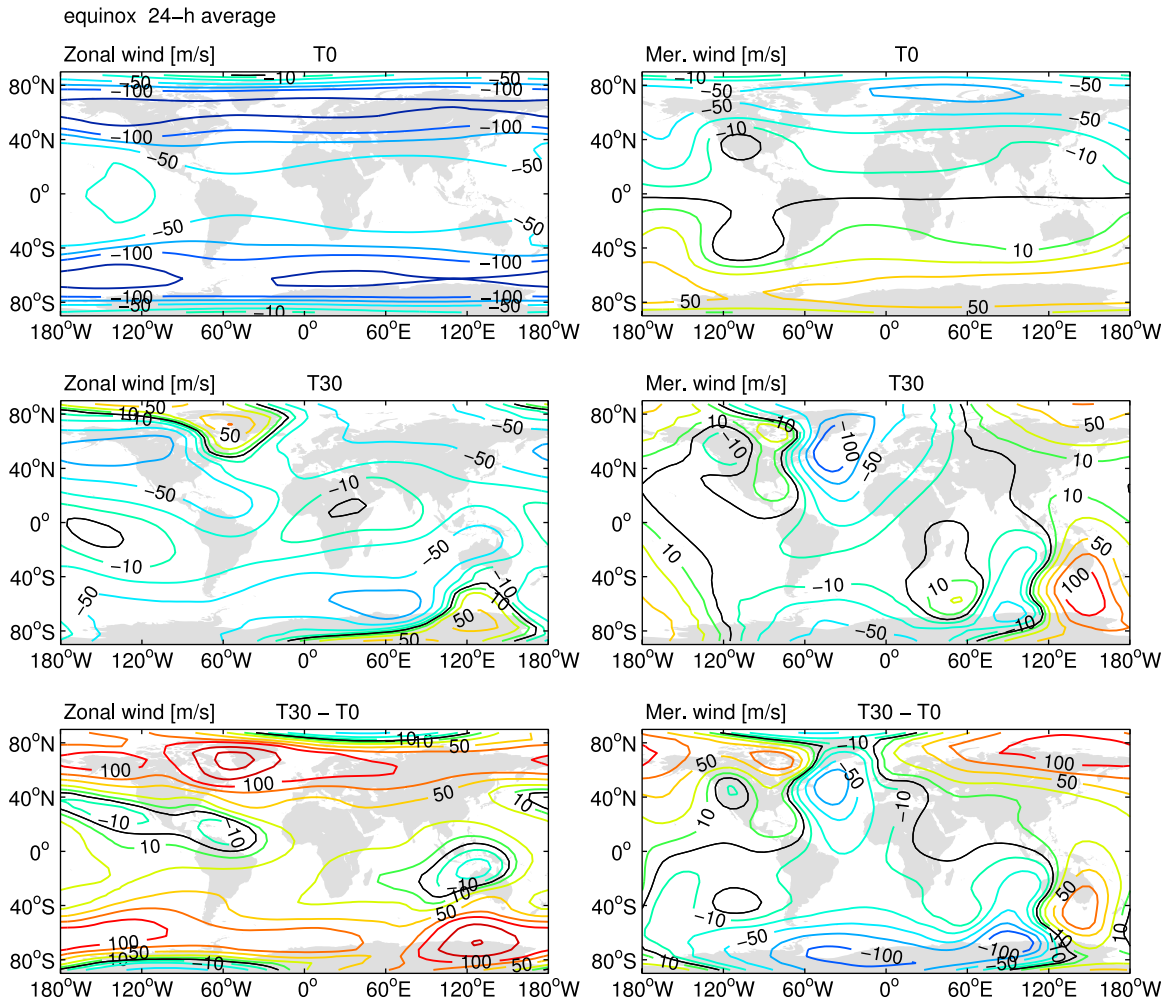

Figure 6. Maps the 24-h mean zonal and meridional wind (m/s) for T0, T30, and the difference (T30-T0) for March equinox and southward IMF. All maps are at a constant pressure level of $3.2 \cdot 10^{-8}$ hPa, corresponding roughly to the level of the F_2 peak height.

4.2. Spatially Varying Responses

[25] A change in the dipole tilt angle does not only affect the temporal variation of the upper atmosphere but also its spatial structure, at least in a geographical reference frame. Such changes are associated with a different mapping of magnetic coordinates to geographic coordinates as the dipole tilt changes. To characterize the spatial effects of changes in tilt angle, we will compare as an example the averages over the last 24 h of the T0 and T30 equinox simulations in some more detail. Responses at solstice, while somewhat different from those at equinox, are formed by the same mechanisms, and will therefore not be shown.

[26] Figure 5 shows maps of the 24-h average Joule heating and temperature for T0, T30, and the difference (T30-T0). Joule heating occurs mainly at high magnetic latitudes because it is associated with the strong ionospheric convection over the polar cap, driven by the magnetosphere. When the locations of the magnetic poles change, the Joule heating follows, as expected. It is also clear that there is less Joule heating in the T30 case than in the T0 case, in correspondence with the results shown in the previous section. The changes in the primary location and the amount of Joule heating cause the temperature structure to change. The temperature increases near the new locations of the magnetic poles, where Joule heating has increased, while it decreases in areas that the magnetic poles have moved away from. However, the increases in temperature do not occur exactly in the same regions where an increase in Joule heating occurs. This is probably due to dynamical adjustment and transport by neutral winds.

[27] The zonal and meridional winds are shown in Figure 6. For the T0 case there are strong westward winds. These arise because the temperature gradients, and therefore the pressure gradients, occur primarily in the meridional direction. Winds will initially blow away from the high-pressure (=high-temperature) areas and are then deflected by the Coriolis effect, resulting in westward winds, or anticyclonic vortices around the poles. As the dipole tilt increases, and the magnetic poles move away from the geographic poles, the pressure maxima and associated anticyclonic vortices tend to follow the displacement of the Joule heating, while also becoming weaker due to the reduction of heating. The direction of the winds therefore changes, in particular near the old and new locations of the magnetic poles. Zonal winds become relatively weaker, and meridional winds

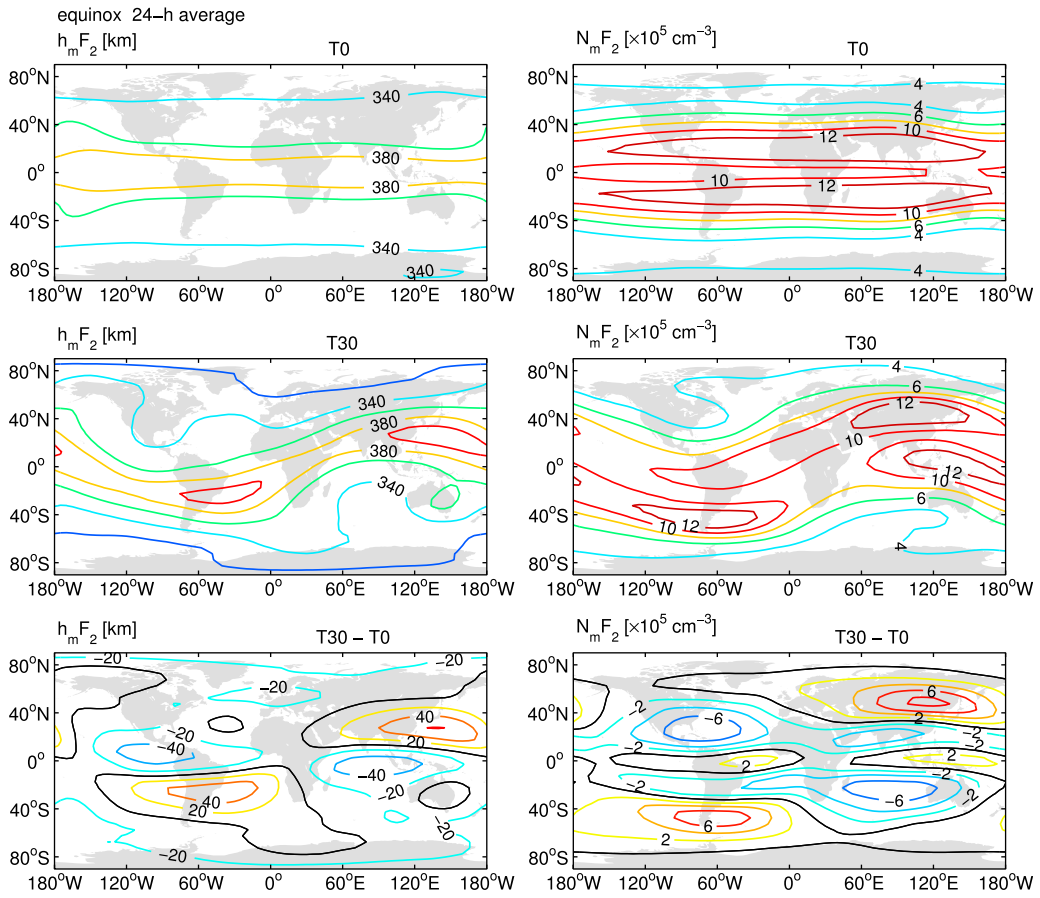

Figure 7. Maps of the 24-h mean height of the F_2 peak, h_mF_2 (km) and the peak electron density of the F_2 layer, N_mF_2 ($\times 10^5$ cm^{-3}) for T0, T30, and the difference (T30-T0) for March equinox and southward IMF.

become relatively stronger as the dipole tilt increases. Changes in ion $\mathbf{E} \times \mathbf{B}$ drifts also have the potential to alter the neutral winds. However, in a 24-h average the ion convection pattern more or less cancels itself out, so that its influence on the 24-h average neutral winds is small.

[28] The changes in the neutral winds modify where most of the changes in temperature occur. For instance, in Figure 5 we can see that regions of increased temperature are displaced equatorward and to the east with respect to the regions of increased Joule heating in both hemispheres. This is probably due to relatively stronger equatorward winds and weaker westward winds for T30 compared to T0.

[29] Figure 7 shows the height of the peak of the F_2 layer, h_mF_2, and the peak density, N_mF_2, for T0, T30, and the difference (T30-T0). Both variables are obviously organized by magnetic latitude. For h_mF_2, the largest values occur at the magnetic equator, while a double-peak structure can be seen in N_mF_2, with maxima on either side of the magnetic equator. For T0, this gives very little longitudinal variation in h_mF_2 and N_mF_2, but as the dipole tilt increases, the original pattern becomes gradually more distorted, showing an undulating shape, which follows magnetic latitudes (compare to Figure 1). This produces an alternating pattern of increases and decreases on either side of the geographic equator.

[30] To determine which processes are responsible for the changes in h_mF_2 and N_mF_2, we show a few other diagnostics for the T30-T0 difference in Figure 8. Figure 8 (top) shows the difference in the O/N_2 ratio, which is a measure of ion production versus ion loss processes. A higher O/N_2 ratio means that relatively less recombination takes place, resulting in larger electron densities and usually a higher N_mF_2. Indeed, the difference patterns in the O/N_2 ratio are reasonably similar to those seen in N_mF_2, which suggests that at least some of the changes in N_mF_2 are due to changes in the O/N_2 ratio. The O/N_2 ratio itself can be related to the neutral wind circulation. Because the meridional winds are mainly directed equatorward, away from the magnetic poles, upwelling occurs at high magnetic latitudes. The air that is brought up is molecular-rich and reduces the O/N_2 ratio in the vicinity of the magnetic poles. In areas of convergent flow (in this case away from the magnetic poles), downwelling takes place, which increases the O/N_2 ratio. Because Joule heating for T30 is less than for T0, the T30-T0 difference of O/N_2 in Figure 8 reflects a reduction of the amplitudes of the O/N_2 equatorial maximum and polar minima, so that the T30-T0 difference tends to be positive at high latitudes and negative at low latitudes, in addition to displaying reductions near the displaced magnetic poles of the T30 case.

[31] Neutral winds can also directly affect the vertical distribution of ionospheric plasma. When blowing along magnetic field lines, horizontal neutral winds drag the plasma up (down) these field lines, which tends to increase (decrease) h_mF_2. In addition, when plasma is moved to higher (lower)

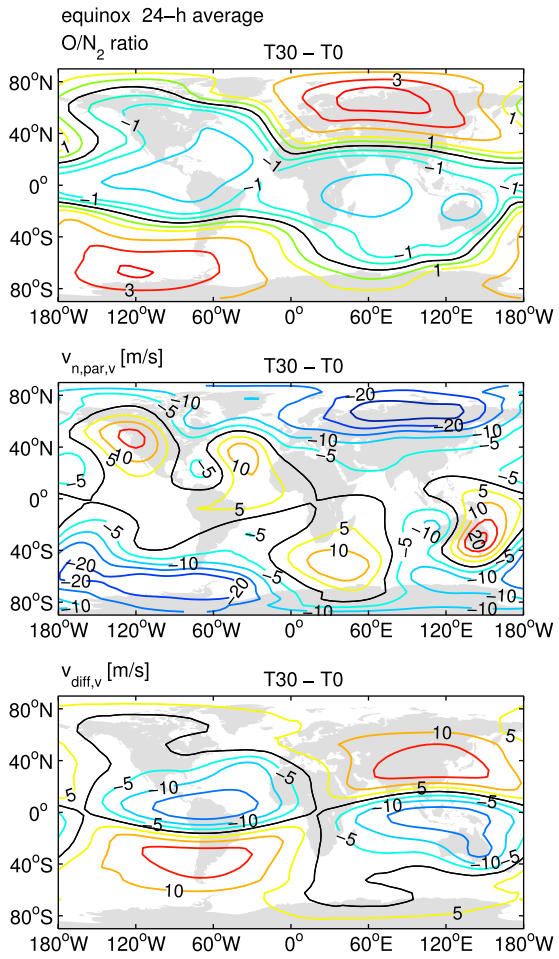

Figure 8. Maps of the difference (T30-T0) of the 24-h mean O/N_2 ratio, the vertical component of the plasma transport by neutral winds along magnetic field lines, $v_{n,par,v}$ (m/s), and the vertical component of the plasma diffusion along magnetic field lines, v_{diff} (m/s) for March equinox and southward IMF. Both velocities are positive upwards. All maps are at a constant pressure level of $3.2 \cdot 10^{-8}$ hPa, corresponding roughly to the level of the F_2 peak height.

altitudes, there is usually less (more) recombination, resulting in an increase (decrease) in N_mF_2. The effect of the horizontal neutral winds on vertical plasma transport can be described by the quantity $v_{n,par,v}$, which is the vertical component of the projection of the horizontal neutral wind parallel to the horizontal component of the magnetic field onto the magnetic field [e.g., *Titheridge*, 1995; *Rishbeth*, 1998; *Cnossen and Richmond*, 2008]. It is defined as

$$v_{n,par,v} = -(V_n \cos\delta + U_n \sin\delta)\sin I \cos I \qquad (2)$$

where U_n and V_n are the zonal and meridional components of the neutral wind velocity, respectively, δ is the magnetic field declination (the angle of the field with respect to magnetic north, positive eastward), and I is the magnetic field inclination (the angle of the field with respect to the horizontal, positive downward). When $v_{n,par,v}$ is positive (negative), this means that ionospheric plasma is dragged up (down) magnetic field lines. Changes in $v_{n,par,v}$ with tilt angle can occur due to changes in the neutral winds as well as due to changes in the declination and inclination of the magnetic field at a given geographic location.

[32] Figure 8 (middle) shows the difference in $v_{n,par,v}$ (T30-T0) at equinox. For T0 (not shown), $v_{n,par,v}$ is positive almost everywhere because the neutral winds that are aligned with the magnetic field (the meridional winds in this case) primarily flow equatorward. On the other hand, for T30, $v_{n,par,v}$ becomes negative at middle to high latitudes in longitudinal sectors away from the magnetic poles and at all longitudes for latitudes >80°, which should produce a decrease in h_mF_2. However, the difference pattern in $v_{n,par,v}$ does not match the pattern seen in h_mF_2. While $v_{n,par,v}$ does have some influence on h_mF_2, most easily noticeable in the 340 km contour of h_mF_2 for the T30 case, it plays a relatively minor role, and is certainly not the main cause of the changes in h_mF_2.

[33] Ionospheric plasma can also be transported along magnetic field lines via diffusion. Gravity is the main driving force behind this, so that the plasma generally diffuses downward along the inclined magnetic field. This acts to decrease h_mF_2 directly and also reduces N_mF_2 by bringing the plasma into a regime where more recombination takes place. Only at very low magnetic latitudes, where the magnetic field is essentially horizontal, plasma diffuses mainly horizontally, away from the magnetic equator. The lack of downward diffusion at low magnetic latitudes is the main reason that h_mF_2 and N_mF_2 are highest near the magnetic equator, while the horizontal diffusion away from the magnetic equator contributes to the slight dip in N_mF_2 right at the equator, resulting in its double-peak structure.

[34] Figure 8 (bottom) shows the difference in the vertical component of the diffusion velocity along magnetic field lines. Because the magnitude of the vertical diffusion velocity depends directly on the inclination of the magnetic field, the diffusion patterns follow magnetic latitudes, with the weakest diffusion always occurring at the magnetic equator. The difference in vertical diffusion velocity therefore resembles a checkerboard pattern: in the longitudinal sector of the magnetic pole in each hemisphere, the downward diffusion is enhanced in that hemisphere and reduced in the other hemisphere. The pattern is very similar to the difference pattern in h_mF_2, except at high latitudes, and somewhat similar to the difference pattern in N_mF_2. It is therefore likely that changes in vertical diffusion play a significant role in causing the changes in h_mF_2 and, to a somewhat lesser extent, in N_mF_2.

4.3. Northward IMF

[35] So far, we have shown results for southward IMF conditions only. Since changes in the Joule heating play a key role in the responses in temperature and neutral winds, we may expect the results to change considerably for northward IMF, when solar wind-magnetosphere coupling is much reduced, and the magnetospheric driving of the high-latitude ionosphere is much weaker. We therefore examine again some of the results for the equinox T0 and T30 cases, but now for northward IMF.

[36] Figure 9 shows the Joule heating and temperature for T0, T30, and the difference (T30-T0) for northward IMF. This can be compared directly to Figure 5, which showed

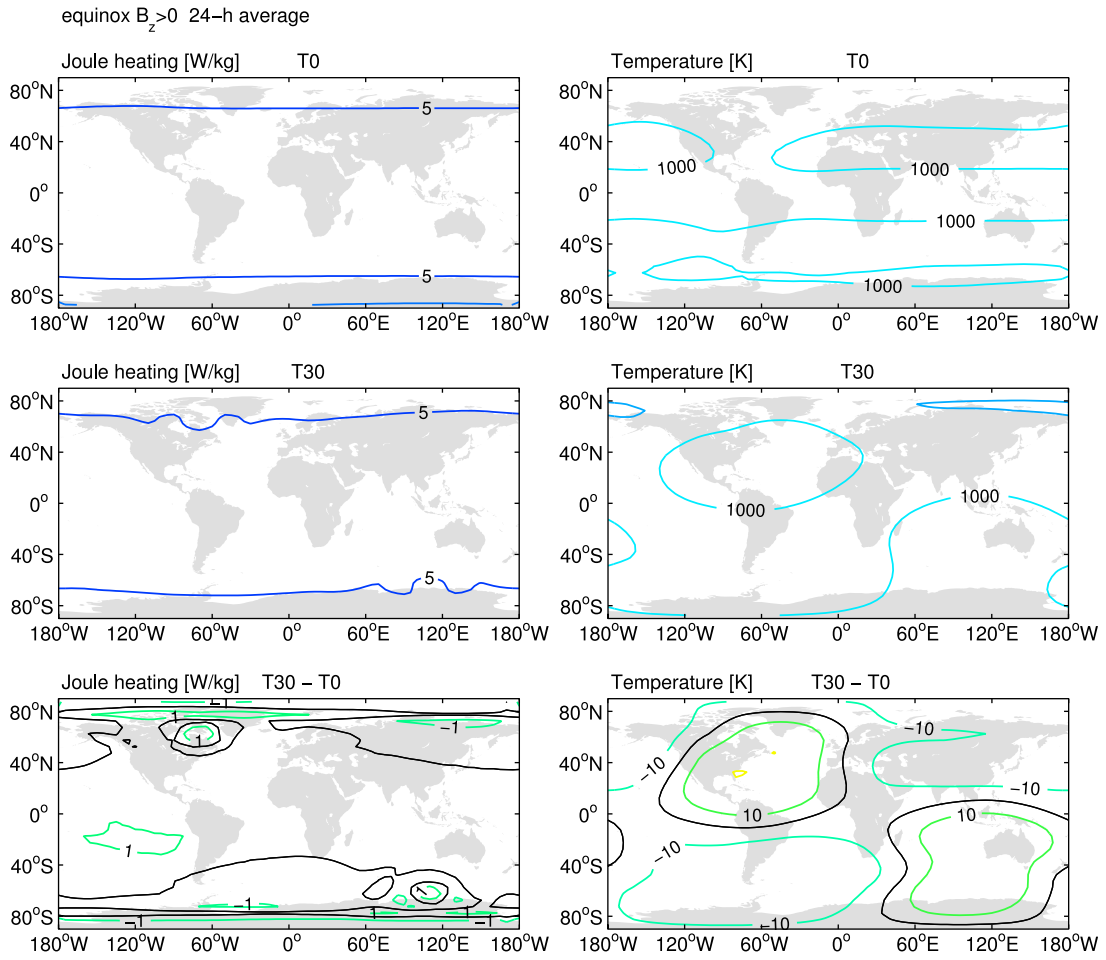

Figure 9. Maps of the 24-h mean Joule heating (W/kg) and temperature (K) for T0, T30, and the difference (T30-T0) for March equinox and northward IMF. All maps are at a constant pressure level of $3.2 \cdot 10^{-8}$ hPa, corresponding roughly to the level of the F_2 peak height.

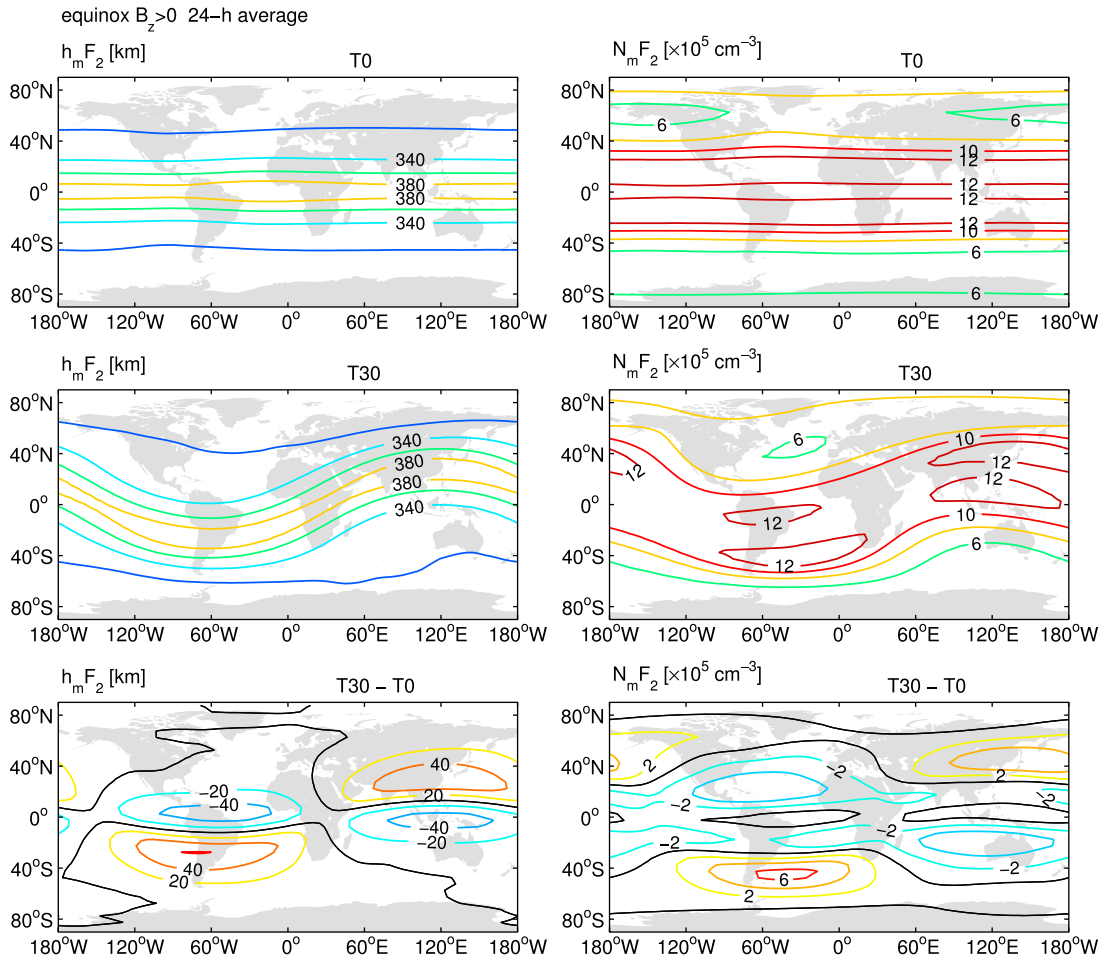

Figure 10. Maps of the 24-h mean height of the F_2 peak, h_mF_2 (km) and the peak electron density of the F_2 layer, N_mF_2 ($\times 10^5$ cm^{-3}) for T0, T30, and the difference (T30-T0) for March equinox and northward IMF. All maps are at a constant pressure level of $3.2 \cdot 10^{-8}$ hPa, corresponding roughly to the level of the F_2 peak height.

the same results for southward IMF. The same contour intervals and color scale were used. It is immediately clear that during northward IMF, the Joule heating is much weaker, and temperatures are reduced, as expected. Because there is generally less Joule heating, changes in its distribution and magnitude from T0 to T30 have less effect on the temperature, but the general patterns are similar to the southward IMF case. The neutral winds, and their changes from T0 to T30, are also much weaker during northward IMF (not shown).

[37] Figure 10 shows maps of h_mF_2 and N_mF_2 for T0, T30, and the difference (T30-T0) during northward IMF. The changes in h_mF_2 with tilt angle are very similar in both strength and structure for northward and southward IMF at low to midlatitudes (compare with Figure 7). This is probably because these changes are produced primarily by changes in the vertical diffusion velocity, which does not depend on high-latitude magnetospheric forcing, and therefore not on the direction of the IMF. At high latitudes, very little change in h_mF_2 is found under northward IMF, while there was a clear decrease in h_mF_2 at high latitudes under southward IMF. This may be associated with strong high-latitude decreases in temperature under southward IMF, which act to lower h_mF_2 through thermal contraction, versus much weaker changes in temperature under northward IMF.

[38] The changes in N_mF_2 with tilt angle are generally smaller, by about a third, under northward than under southward IMF, but similar in spatial structure. In section 4.2, we suggested that both changes in the O/N_2 ratio and changes in the vertical component of the plasma diffusion along magnetic field lines could have contributed to the changes in N_mF_2 under southward IMF. The difference in these variables between T30 and T0 under northward IMF conditions is shown in Figure 11. The changes in vertical diffusion velocity are nearly the same for both IMF conditions (compare Figures 8 (bottom) and 11 (bottom)), so these must have contributed more or less equally in both cases. Changes in the O/N_2 ratio, however, are much smaller under northward IMF (compare Figures 8 (top) and 11 (top)) because there is much less change in neutral winds. This can explain why the changes in N_mF_2 are also weaker in this case. The results for both IMF conditions combined also suggest that changes in the O/N_2 ratio are responsible for about a third of the

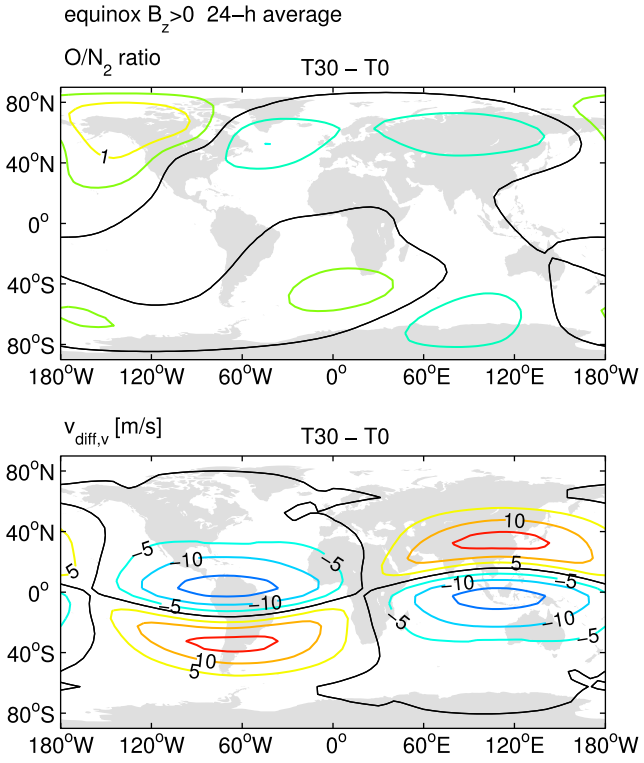

Figure 11. Maps of the difference (T30-T0) of the 24-h mean O/N_2 ratio and the vertical component of the plasma diffusion along magnetic field lines, v_{diff} (m/s) for March equinox and southward IMF. The plasma diffusion velocity is positive upwards. Both maps are at a constant pressure level of $3.2 \cdot 10^{-8}$ hPa, corresponding roughly to the level of the F_2 peak height.

changes in N_mF_2 seen under southward IMF, with the remainder due to changes in vertical diffusion.

5. Discussion and Conclusions

[39] In section 2 we introduced three ways in which a change in dipole tilt angle can affect the MIT system: changes in the amount of Joule heating through variations in solar wind-magnetosphere coupling efficiency, changes in the geographic distribution of Joule heating and magnetospherically driven ion convection patterns through changes in magnetic pole positions, and changes in vertical plasma transport through changes in the inclination of the magnetic field at a given geographic location. We have shown that each of these mechanisms does indeed contribute to the response of the MIT system to a change in tilt angle.

[40] The dipole tilt angle modulates the diurnal variation in solar wind-magnetosphere coupling efficiency, which results in an increase in diurnal variation in cross-polar cap potential and Joule heating with increasing tilt angle. At equinox, an increase in tilt angle leads to a lower cross-polar cap potential and less Joule heating averaged over 24 h. At solstice, the 24-h average cross-polar cap potential slightly increases with increasing tilt angle up to a tilt of 20° but decreases when the tilt angle is increased further. The Joule heating behaves similarly in summer, while in winter the Joule heating keeps increasing with increasing tilt angle up to a tilt of 40° before starting to decrease as well. Seasonal differences in cross-polar cap potential and Joule heating are reduced with increasing tilt angle. Changes in both the average magnitude and the geographic distribution of Joule heating cause changes in the temperature and neutral winds. Changes in temperature with tilt angle may contribute to changes in h_mF_2, in particular at high latitudes, while changes in neutral winds cause changes in the O/N_2 ratio, which affects N_mF_2.

[41] The effects described above are mainly important when solar wind-magnetosphere coupling is strong, as it is during southward IMF. During northward IMF, Joule heating is very weak to begin with, so that any changes in Joule heating are also small and have little effect. While we only investigated the effect of the IMF B_z component on the results, it is likely that changes in the background level of Joule heating by other factors will affect the results similarly. We therefore expect that the effects of a change in tilt angle via Joule heating-related mechanisms will, in general, be most noticeable during disturbed conditions, such as during magnetospheric (sub)storms.

[42] In contrast, changes in inclination affect the ionosphere in more or less the same way, regardless of the solar wind conditions and the state of the magnetosphere. We find that in particular the effect of the inclination on the vertical component of the diffusion of ionospheric plasma along magnetic field lines is important in causing changes in h_mF_2 and N_mF_2 at low to midlatitudes. Changes in the vertical component of the plasma velocity along magnetic field lines induced by horizontal neutral winds, i.e., changes in $v_{n,par,v}$, are much less important.

[43] We note that in reality, the Earth's magnetic field is not purely dipolar, and when changes in the magnetic field take place, it is usually not just the main dipole component that is changing. The NH and SH magnetic poles do therefore not necessarily move coherently, and changes in inclination can occur locally. Because of this, responses to more realistic changes in magnetic field orientation are likely to look somewhat different. However, we expect the mechanisms by which changes in magnetic pole position or inclination affect the MIT, as identified here, to remain valid. We will use this information in a future study to analyze the effects of more realistic, historical magnetic field changes on the MIT.

[44] Finally, the results of our study may also have implications for the present-day, as the NH and SH magnetic poles, where the magnetic field inclination equals ±90°, have different offsets with respect to the Earth's rotation axis, with the offset in the SH being considerably larger (~25°) than in the NH (~5°). *Förster et al.* [2008] argued that this difference could explain the larger standard deviation in high-latitude neutral winds in the SH compared to the NH they observed in a statistical study of data from the Challenging Minisatellite Payload (CHAMP). We slightly modify this idea and suggest that it is really the position of the invariant poles, where invariant latitude = 90°, that matters because the auroral ovals are more or less centered on these poles rather than the magnetic poles. However, the positions of the invariant poles also show a larger offset from the rotation axis in the SH (~16°) than in the NH (~8°), so that the SH should still show behavior associated with a larger tilt angle. The larger standard deviations we find for larger dipole tilt angles thus lend support for the idea that the larger standard

deviations found in the SH by *Förster et al.* [2008] are due to NH/SH asymmetry in the Earth's magnetic field, although we did not show results for neutral winds specifically.

[45] *Bruinsma et al.* [2006] used data from both CHAMP and the Gravity Recovery and Climate Experiment (GRACE) to study the response of the upper atmosphere to the geomagnetic storm of 20–21 November 2003. They find stronger responses in density and plasma drifts in the SH than in the NH, and attribute this to the higher ionospheric conductance in the SH, mostly due to the time of year (near December solstice), but aided by the enhanced offset of the magnetic pole in the SH. According to them this should facilitate coupling with the solar wind. Our results indicate that solar wind-magnetosphere coupling is in fact reduced for a larger tilt angle, in nearly the same way for the summer and winter hemispheres, but we do confirm that Joule heating is larger in the summer hemisphere at ~10–11 UT, when the observations were made. However, this is a direct effect of the difference in conductance between the hemispheres, and this difference is mainly a seasonal effect. The tilt angle has little influence at 10–11 UT, with conductances for T0-T20 being all very similar at that time (see Figure 2b).

[46] **Acknowledgments.** We thank Jiuhou Lei for help with calculating the vertical component of the plasma diffusion velocity and two anonymous reviewers for helpful comments. Part of this work was supported by NASA grants NNH07AF041 and NNX08AG09G and NSF CEDAR grant ATM-0836386. The National Center for Atmospheric Research is sponsored by the National Science Foundation.

[47] Robert Lysak thanks the reviewers for their assistance in evaluating this paper.

References

Amit, H., and P. Olson (2008), Geomagnetic dipole tilt changes induced by core flow, *Phys. Earth Planet. Inter.*, *166*(3–4), 226–238, doi:10.1016/j.pepi.2008.01.007.

Bruinsma, S., J. M. Forbes, R. S. Nerem, and X. Zhang (2006), Thermospheric density response to the 20–21 November 2003 solar and geomagnetic storm from CHAMP and GRACE accelerometer data, *J. Geophys. Res.*, *111*, A06303, doi:10.1029/2005JA011284.

Cnossen, I., and A. D. Richmond (2008), Modelling the effects of changes in the Earth's magnetic field from 1957 to 1997 on the ionospheric hmF2 and foF2 parameters, *J. Atmos. Sol. Terr. Phys.*, *70*, 1512–1524, doi:10.1016/j.jastp.2008.05.003.

Cnossen, I., A. D. Richmond, M. Wiltberger, W. Wang, and P. Schmitt (2011), The response of the coupled magnetosphere-ionosphere-thermosphere system to a 25% reduction in the dipole moment of the Earth's magnetic field, *J. Geophys. Res.*, *116*, A12304, doi:10.1029/2011JA017063.

Cnossen, I., A. D. Richmond, and M. Wiltberger (2012), The dependence of the coupled magnetosphere-ionosphere-thermosphere system on the Earth's magnetic dipole moment, *J. Geophys. Res.*, *117*, A05302, doi:10.1029/2012JA017555.

Förster, M., S. Rentz, W. Köhler, H. Liu, and S. E. Haaland (2008), IMF dependence of high-latitude thermospheric wind pattern derived from CHAMP cross-track measurements, *Ann. Geophys.*, *26*, 1581–1595, doi:10.5194/angeo-26-1581-2008.

Jacobs, J. A. (1984), *Reversals of the Earth's Magnetic Field*, 230 pp., Adam Hilger Ltd, Bristol, UK.

Korth, H., B. J. Anderson, M. J. Wiltberger, J. G. Lyon, and P. C. Anderson (2004), Intercomparison of ionospheric electrodynamics from the Iridium constellation with global MHD simulations, *J. Geophys. Res.*, *109*, A07307, doi:10.1029/2004JA010428.

Lyon, J. G., J. A. Fedder, and C. M. Mobarry (2004), The Lyon-Fedder-Mobarry (LFM) global MHD magnetospheric simulation code, *J. Atmos. Sol. Terr. Phys.*, *66*(15–16), 1333–1350, doi:10.1016/j.jastp.2004.03.020.

McHarg, M., F. Chun, D. Knipp, G. Lu, B. Emery, and A. Ridley (2005), High-latitude Joule response to IMF inputs, *J. Geophys. Res.*, *110*, A08309, doi:10.1029/2004JA010949.

Merkin, V. G., and J. G. Lyon (2010), Effects of the low-latitude ionospheric boundary condition on the global magnetosphere, *J. Geophys. Res.*, *115*, A10202, doi:10.1029/2010JA015461.

Richmond, A. D., E. C. Ridley, and R. G. Roble (1992), A thermosphere/ionosphere general circulation model with coupled electrodynamics, *Geophys. Res. Lett.*, *19*(6), 601–604, doi:10.1029/92GL00401.

Rishbeth, H. (1998), How the thermospheric circulation affects the ionospheric F2-layer, *J. Atmos. Sol. Terr. Phys.*, *60*, 1385–1402, doi:10.1016/S1364-6826(98)00062-5.

Roble, R. G., E. C. Ridley, A. D. Richmond, and R. E. Dickinson (1988), A coupled thermosphere/ionosphere general circulation model, *Geophys. Res. Lett.*, *15*(12), 1325–1328, doi:10.1029/GL015i012p01325.

Siscoe, G. L., and L. Christopher (1975), Effects of geomagnetic dipole variations on the auroral zone locations, *J. Geomagn. Geoelectr.*, *27*, 485–489, doi:10.5636/jgg.27.485.

Titheridge, J. E. (1995), Winds in the ionosphere - A review, *J. Atmos. Terr. Phys.*, *57*(14), 1681–1714, doi:10.1016/0021-9169(95)00091-F.

Wang, W., M. Wiltberger, A. G. Burns, S. C. Solomon, T. L. Killeen, N. Maruyama, and J. G. Lyon (2004), Initial results from the coupled magnetosphere-ionosphere-thermosphere model: Thermosphere-ionosphere responses, *J. Atmos. Sol. Terr. Phys.*, *66*(15–16), 1425–1441, doi:10.1016/j.jastp.2004.04.008.

Wang, W. B., J. H. Lei, A. G. Burns, M. Wiltberger, A. D. Richmond, S. C. Solomon, T. L. Killeen, E. R. Talaat, and D. N. Anderson (2008), Ionospheric electric field variations during a geomagnetic storm simulated by a coupled magnetosphere ionosphere thermosphere (CMIT) model, *Geophys. Res. Lett.*, *35*, L18105, doi:10.1029/2008GL035155.

Wiltberger, M., W. Wang, A. G. Burns, S. C. Solomon, J. G. Lyon, and C. C. Goodrich (2004), Initial results from the coupled magnetosphere ionosphere thermosphere model: Magnetospheric and ionospheric responses, *J. Atmos. Sol. Terr. Phys.*, *66*(15–16), 1411–1423, doi:10.1016/j.jastp.2004.03.026.

Wiltberger, M., R. S. Weigel, W. Lotko, and J. A. Fedder (2009), Modeling seasonal variations of auroral particle precipitation in a global-scale magnetosphere-ionosphere simulation, *J. Geophys. Res.*, *114*, A01204, doi:10.1029/2008JA013108.

Zieger, B., J. Vogt, K.-H. Glassmeier, and T. I. Gombosi (2004), Magnetohydrodynamic simulation of an equatorial dipolar magnetosphere, *J. Geophys. Res.*, *109*, A07205, doi:10.1029/2004JA010434.